crystals

MDPI

Article

Role of Hydrodynamics, Li^+ Addition and Transformation Kinetics on the Formation of Plate-Like {001} Calcite Crystals

Nives Matijaković Mlinarić [1], Jasminka Kontrec [1], Branka Njegić Džakula [1], Giuseppe Falini [2] and Damir Kralj [1,*]

[1] Laboratory for Precipitation Processes, Division of Materials Chemistry, Ruđer Bošković Institute, P. O. Box 180, HR-10002 Zagreb, Croatia; nives.matijakovic@irb.hr (N.M.M.); jasminka.kontrec@irb.hr (J.K.); bnjeg@irb.hr (B.N.D.)

[2] Dipartimento di Chimica "Giacomo Ciamician", Alma Mater Studiorum—Universitá di Bologna, via Selmi 2, 40126 Bologna, Italy; giuseppe.falini@unibo.it

* Correspondence: kralj@irb.hr; Tel.: +385-1-468-0207

Abstract: Plate-like calcite crystals with expressed unstable {001} planes are interesting research model for investigations of interfacial interactions of different additive molecules, but also the crystal growth mechanisms. The aim of this study is to reproducibly prepare a significant amount of well-defined plate-like calcite crystals and to investigate the critical experimental parameters. Thus, in precipitation system $c(NaHCO_3) = c(CaCl_2) = 0.1$ mol dm^{-3}, the influence of hydrodynamic parameters (mode of mixing of the reaction components) and a presence of lithium ions Li^+ within a wide range of concentrations, 0.0 mol dm^{-3} < $c(Li^+)$ < 1.0 mol dm^{-3}, have been studied. In addition, the kinetics of the solution mediated transformation of the initially formed metastable polymorph, vaterite, were followed in order to reproducibly describe the formation of stable calcite with expressed unstable morphology. The results indicate that the plate-like calcite is formed predominantly when the ultrasound irradiation is applied at $c(Li^+) \geq 0.3$ mol dm^{-3}. On the other hand, when the magnetic and mechanical stirring are applied at higher Li^+ concentrations, truncated rhombohedral crystals in a mixture with plate-like crystals are obtained. It was also found that the Li^+ addition significantly prolonged the transformation, mainly by inhibiting the crystal growth of calcite.

Keywords: {001} plane; calcite; lithium ions; kinetic of transformation; stirring effect; calcite formation

Citation: Matijaković Mlinarić, N.; Kontrec, J.; Njegić Džakula, B.; Falini, G.; Kralj, D. Role of Hydrodynamics, Li^+ Addition and Transformation Kinetics on the Formation of Plate-Like {001} Calcite Crystals. *Crystals* **2021**, *11*, 250. https://doi.org/10.3390/cryst11030250

Academic Editor: Sławomir J. Grabowski

Received: 8 February 2021
Accepted: 24 February 2021
Published: 28 February 2021

1. Introduction

Calcium carbonate crystals, particularly those of calcite, are interesting model systems for studying the interfacial interactions on crystal planes, namely, for any detailed analysis of crystal growth kinetics and mechanisms, or investigation of basic molecular interactions that may happen at the solid-liquid interfaces. To perform this investigation, crystal seed material uniform in size and with well exposed crystallographic planes is necessary [1–6]. Calcite crystals of different morphologies may be precipitated from aqueous solutions at different technological or environmental conditions or during the biomineralization processes. Biologically produced calcium carbonate appears in many different shapes and morphologies and typically builds exoskeletons of phytoplankton; sponges; echinoderms; invertebrates (corals, mollusks and crustaceans) or eggshells, but they also occur in the inner ear as the gravity receptor (otoliths) in mammals and fishes [7]. The morphology and shape of these highly ordered organic-inorganic composites are controlled by biologically active macromolecules that interact with specific crystal planes during their nucleation and crystal growth [8]. These processes have been extensively studied on the molecular level in order to understand the respective interactions and mechanisms of preparation of highly functionalized composite materials [9–16].

Regular plate-like calcite crystals are a relatively atypical morphology with expressed {001} crystallographic faces. They can be found in the brittle stars (echinoderms) in form

of micro lens arrays in light receptor systems [17,18]. The plate-like calcite crystals can be produced in vitro as well, by calcium carbonate precipitation in the presence of Li^+ ions [1,19–21]. At that, the expression of the {001} faces is enhanced by higher $c(Li^+)/c(Ca^{2+})$ ratios [19,21–26]. In an additive-free calcite/solution systems, the {001} faces have lower stability compared to {104} rhombohedral faces, as shown by in silico experiments [27]. The relative stability of the {001} faces is actually a destabilization of the {104} planes by Li^+ [25,27].

The typical experimental parameters considered during the preparation of crystals of different morphologies are the concentration of additives, pH, temperature or supersaturation, but different stirring modes (hydrodynamics) can significantly influence the phase ratio, morphology and crystal size distribution, as demonstrated for different model systems of slightly soluble ionic salts [2,12,28–35]. However, it was also shown for the calcium carbonate precipitation systems that ultrasonic irradiation is an important experimental parameter that can influence precipitation by accelerating it and in chemically simple systems typically leads to formation of the unstable polymorph, vaterite [36–38].

This study aims to investigate the role of different thermodynamic and hydrodynamic factors on the formation of plate-like calcite crystals with well-developed {001} crystal faces in the presence of Li^+. The working hypothesis is that the Li^+ concentration is not the only parameter that controls the stabilization of {001}. Thus, the concentration of Li^+, $(c(Li^+)/c(Ca^{2+})$, as well as the stirring modes (stirring with a magnetic bar, mechanical blade and pulse ultrasonic irradiation) are considered as key parameters for inducing formation of specific morphologies. In addition, the kinetics of transformation of vaterite to calcite were analyzed and correlated with the experimental parameters.

2. Materials and Methods

2.1. Preparation of Plate-Like Crystal Seed

Calcium carbonate precipitation was initiated by mixing equal volumes (200 cm^3) of solutions containing LiCl and $CaCl_2$ with $NaHCO_3$ solution, all freshly prepared. Deionized water (conductivity < 0.055 μS cm^{-1}) and analytical grade chemicals LiCl (Fluka, Buchs, Switzerland), $CaCl_2 \cdot 2\,H_2O$ (Acros organics, Geel, Belgium) and $NaHCO_3$ (Sigma Aldrich, St. Louis, MS, USA) were used for the preparation of the solutions. The solutions were thermostated at 298 K. The Li^+ concentration was varied in the range $0.0 < c(Li^+) < 1.0$ mol dm^{-3} while the $NaHCO_3$ and $CaCl_2$ concentrations were 0.1 mol dm^{-3} in all precipitation systems. The experiments were performed by simultaneous and fast mixing of $CaCl_2$/LiCl solutions into the $NaHCO_3$ solution. The model experiments were carried out in the absence of LiCl. The precipitation systems were stirred by using either, (a) a Teflon-coated magnetic stirring bar (MAG), (b) mechanical propeller (MECH) or (c) pulse ultrasonic irradiation* (US). The solutions were initially stirred for 60 min at a constant rate by the magnetic and mechanic stirrer, while the pulse sonication process was applied for 10 min. After the stirring period, the systems were gently shacked for five days in order to avoid unintentional breaking of formed plate-like crystals. Mechanical stirring was conducted by flat-blade stirrer, positioned just above the bottom of the glass reactor, with two perpendicular blades rotating at 200 rpm. The lower blade is 50 mm in diameter, while the upper blade (20 mm diameter) was perpendicular and separated by 20 mm. The initial magnetic stirring was achieved by 20 mm diameter stirrer rotating at 400 rpm. The sonication was initiated in the $NaHCO_3$ solution before addition of $CaCl_2$/LiCl solution, by using Branson Sonifier 250 (20 kHz frequency) [1]. The applied power output was set at 8 W. The ultrasonic horn (diameter 5 mm) was immersed in the center of the reaction vessel, 5 cm above the bottom. The precipitate has been sampled at regular time intervals, starting immediately at the end of the initial stirring period and during the following 5 days. The suspension (10 cm^3) was filtered through a membrane filter (0.22 μm) and the precipitate was dried at 100 °C for one hour. The composition of dry samples has been determined by FT-IR spectroscopy, X-ray powder diffraction (XRD) and ion chromatography. IR spectra were recorded on the FT-IR TENSOR

II (Bruker, Billerica, MA, USA) in the 400–4000 cm^{-1} region using the KBr pellet technique. X-ray powder diffractograms have been collected on the Philips X'Celerator diffractometer (Malvern, United Kingdom) in the scan range $20° \leq 2\ \theta \leq 70°$ with the step size $2\theta = 0.05°$ and measuring the time of 120 s per step. The morphology of crystal samples was determined by FEG SEM Hitachi 6400 (Tokyo, Japan) and Phenom model G2 scanning electron microscope (Eindhoven, The Netherlands) operating in low voltage mode, without coating. The Li^+ ion content in solution and precipitate was determined by Dionex ICS—1100 ion chromatograph (Sunnyvale, CA, USA) fitted with SC16 Analytical Column and using MSA eluent (30 mmol dm^{-3}). The particle size distribution of obtained samples was determined using Image J software [39], while the reference samples were additionally analyzed by an electronic particle counting device (Coulter Counter Multisizer II, Coulter, West Lafayette, IL, USA).

2.2. Precipitation Kinetic (Transformation, Crystal Growth and Dissolution)

The kinetic of calcium carbonate transformation was investigated in the magnetically stirred systems identical to those used for plate-like calcite preparation: V = 400 cm^3, $c_i(NaHCO_3) = c_i(CaCl_2)$ = 0.1 mol dm^{-3}, while the initial LiCl concentrations varied in the range ($0.0 < c(LiCl) < 0.3$ mol dm^{-3}). Initially, the spontaneous and fast precipitation of $CaCO_3$ precursors was observed, and the pH was continuously measured until no changes could be observed and no vaterite could be detected.

The kinetics of the vaterite dissolution were conducted in magnetically stirred systems, undersaturated with respect to vaterite and prepared by mixing bicarbonate and calcium solutions: V = 400 cm^3, $c_i(NaHCO_3) = c_i(CaCl_2)$ = 0.058 mol dm^{-3}, $c(HCl) = c(NaCl)$= 0.042 mol dm^{-3} and ($0.0 < c(LiCl) < 0.3$ mol dm^{-3}). The vaterite crystals used in these experiments were obtained from the US model system, and isolated after 10 min of sonication and dried at 100 °C for one hour. The prepared vaterite crystals seed (m = 400 mg) were dispersed in saturated $CaCO_3$ solution (500 µL), homogenized and rapidly introduced into magnetically stirred undersaturated solution in order to start the dissolution process. The pH was continuously measured until the apparent equilibrium for vaterite was obtained.

The kinetics of the calcite and vaterite crystal growth were investigated in the magnetically stirred, metastable precipitation systems, supersaturated with respect to both polymorphs: V = 400 cm^3, $c_i(NaHCO_3) = c_i(CaCl_2)$ = 0.075 mol dm^{-3}, $c(HCl) = c(NaCl)$= 0.025 mol dm^{-3} and ($0.0 < c(LiCl) < 0.3$ mol dm^{-3}). The growth process was initiated by the fast inoculation of supersaturated solutions, with previously prepared crystal seed (rhombohedral calcite (m = 50 mg) [40] or vaterite (m = 400 mg), each dispersed in a saturated calcite solution (500 µL). The pH was continuously measured until the apparent equilibrium for vaterite or calcite was obtained.

2.3. Treatment of Data

The amount of vaterite dissolved during the dissolution process was calculated on based on the measured pH and initial concentrations of the reactants. At that, the respective dissolved ionic species, equilibrium constants and mass balance equations were considered, as described previously [41]. The dissolution rate was determined by subtracting the calculated dissolved amount and corresponding volume of vaterite (V), from the mass and corresponding initial volume of vaterite seed added in the solution (V_o), particle number density and the average initial diameter of vaterite spheres (r_0 = 1 µm), as determined by SEM. The average radius of the vaterite particles at any moment of the process was calculated:

$$r = (3V_t/4\pi N)^{1/3} \quad (1)$$

where N is the particle number density and V_t is the volume of the precipitate calculated using the mass and density of the precipitate at time t ($V_t = V_o - V$). Using numerical differentiation of r as a function of t, the dissolution rate dr/dt was determined and different dissolution models, in which linear growth rates are function of undersaturation,

have been tested. The best fit was obtained by assuming that the diffusion of ions away from the crystal surface is described by the relation:

$$dr/dt = D \cdot V_m \cdot (c_S - c)/r \quad (2)$$

In this expression, D is the diffusion coefficient, $(c_S - c)$ is the absolute undersaturation, V_m is the specific molar volume, while c_s is calculated solubility of vaterite. In order to estimate the influence of Li^+ on the vaterite dissolution process, the diffusion coefficients were determined for different Li^+ concentrations. Detailed description of calculation procedure can be found in the literature [41].

The amount of calcite or vaterite precipitated during the seeded crystal growth, was determined by subtraction of the calculated total dissolved concentration of calcium carbonate at time t, from the initial total concentration, as described previously [42]. The rate of the crystal growth process was determined by the addition of the calculated dissolved amount of calcite or vaterite to the initial mass of respective crystal seed in the solution, particle number density and the average initial linear dimension of the seed particle (r = 1 µm for vaterite and, l = 1 µm for calcite). The length of calcite rhombohedrons at each moment of the process was calculated:

$$l = (V_t/N)^{1/3} \quad (3)$$

where V_t is the volume of the precipitate calculated using the mass and density of the precipitate at time t ($V_t = V_o - V$) and N is the particle number density. The growth rate, dl/dt, was determined by numerical differentiation and different crystal growth mechanisms (growth controlled by bulk diffusion, growth on screw dislocation, surface nucleation controlled growth) and the mechanisms were tested by correlating the rate with different expressions of supersaturation:

$$\text{Diffusion controlled growth:} \quad dl/dt = D \cdot V_m \cdot (c - c_S)/l \quad (4)$$

$$\text{Growth on screw dislocation:} \quad dl/dt = k_{ln} \cdot ((c - c_S) - 1) \cdot \ln(c/c_S) \quad (5)$$

$$\text{Surface nucleation growth:} \quad dl/dt = k_e \cdot (c/c_S)^{7/6} \cdot ((c/c_S) - 1))^{2/3} (\ln(c/c_S))^{1/6} \cdot \exp(-K_e/\ln(c/c_S)) \quad (6)$$

In the above expressions, k_x is a respective growth rate coefficient, $(c - c_s)$ is absolute supersaturation, c/c_s is relative supersaturations, while c_s is a solubility of respective polymorph. The best linear fit of the experimental data for Equations (4), (5) or (6) indicate the dominant crystal growth mechanism. A brief derivation of Equations (4)–(6) is provided in Table S1 [43]. The influence of Li^+ concentrations on the growth rate mechanisms and kinetics were determined as well, by testing the respective kinetics.

3. Results and Discussion

The principal intention of this study was to determine the influence of different experimental parameters, predominantly the initial concentration of Li^+ and mode of stirring on the preparation of plate-like calcite crystals with dominant {001} faces. The initial concentration of calcium and carbonate ions was relatively high and consequently a mixture of polymorphs and amorphous precursor phases were observed at the early stages of precipitation. Therefore, the kinetics of transformation from vaterite to calcite were analyzed in detailed and the role of the kinetics was correlated with other parameters considered relevant for expression of a specific morphology.

3.1. Structural Analysis

The structural analyses of the precipitate formed in the MAG, MECH or US systems with increasing Li^+ concentrations and isolated after five days of aging, as determined by XRD and FTIR analyses, showed the predominant presence of calcite. However, some

residues of vaterite were observed only in the US system with the highest Li^+ content (Figures S1–S5 and Tables S2–S4). In all the systems the formation of Li_2CO_3 was not been observed, which could be expected due to the solution undersaturation with respect to lithium carbonate ($S_{Li2CO3} < 0.39$). The literature data showed that in similar systems no precipitation of Li_2CO_3 could be expected due to the lack of homogeneous distribution of Li^+ during calcium carbonate formation [44]. The results of the distribution of polymorphs in the initially formed precipitate, but also the precipitate isolated during the aging process and at different lithium concentrations are shown in Figure 1. At the beginning of the ageing process (immediately after termination of initial stirring of one h) the amount of calcite is typically higher in the MECH than in the MAG model systems (no Li^+) (Table S3), which is consistent with some previous results that showed the promotion of the vaterite formation in the magnetically stirred systems [42]. At that, stirring with a magnetic bar caused an abrasive action on the glass, thus causing the predominant nucleation of metastable solid phases, like calcium oxalate trihydrate or vaterite [45]. Similarly, the ultrasonic irradiation leads to the preferential nucleation of metastable solid phases as well, as a consequence of a higher energy input in the supersaturated solutions of slightly soluble calcium salts, like carbonates or oxalates [38,46] (US data shown in Table S3 was reported previously [1].

In addition to the stirring mode, the presence of Li^+ also significantly influenced the changes of the polymorphic composition of the precipitate at early stages of process. Thus, the increase of the initial $c(Li^+)$ in each system and at specific ageing period, resulted in drastic decrease of calcite content in a mixture with vaterite, as could be seen in Figure 1. It could also be observed that the increased $c(Li^+)$ caused the retardation of vaterite transformation to stable calcite, which could be explained either by slower vaterite dissolution or the slower calcite growth, as indicated previously [1]. Thus, in the MAG system, the complete transformation of vaterite in the presence of 0.7 or 1.0 mol dm^{-3} Li^+ terminated after approximately four to five days, while the addition of 0.1 mol dm^{-3} Li^+ stabilized vaterite just for two days. On the other hand, in the MECH system and $c(Li^+)$ = 1.0 mol dm^{-3}, vaterite completely transformed after two days of aging.

3.2. Particle Size Distribution

The mode of stirring also influenced the crystal size distribution of calcite, which was determined at the end of transformation process. The average particle size distributions of typical samples prepared with different initial Li^+ concentrations, different stirring modes and after five days of aging are shown in Figure 2 and Figures S6–S9. It could be seen that in model systems (absence of lithium ions) and at all stirring modes applied, unimodal and relatively narrow particle size distributions were obtained. Thus, the lowest mean crystal size was observed in the US system, about 9 $\pm$ 1.7 μm, in comparison to 14 $\pm$ 2.4 μm and 18 $\pm$ 3.7 μm as observed in the MECH or MAG systems, respectively. The applied high intensity ultrasonic irradiation promotes the uniform size distribution and lower mean size, as a result of the formation of vapor-filled cavities and local increase of temperature caused by their collapsing. Such spots increase the nucleation rate and corresponding increase of the particle number [31,47–49]. On the other hand, in the systems with $c(Li^+)$ = 0.3 mol dm^{-3}, the average size of calcite crystals obtained in the US system was higher than in the respective MECH and MAG systems (28 μm > 14 μm > 14 μm). However, at the highest Li^+ concentration applied, bimodal and much broader size distributions were obtained in all systems, which could be a consequence of appearance of additional morphologies, particle aggregation, or even a presence of non-transformed vaterite particles. Figure S10 shows the average crystal size as a function of the Li^+ concentration, for all mixing systems.

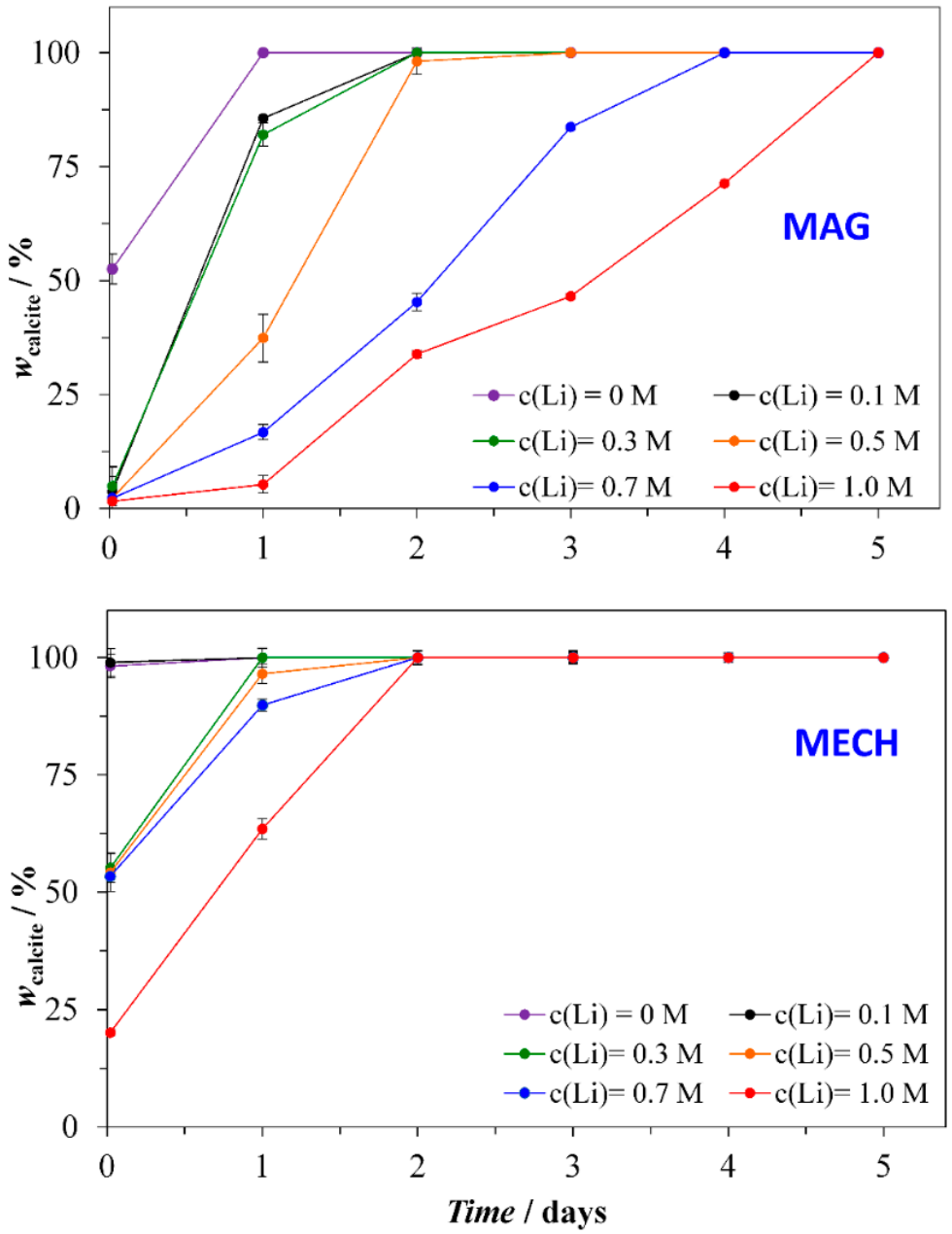

Figure 1. Amount of calcite in the precipitate during the transformation process in the systems, $c_i(CaCl_2) = c_i(NaHCO_3) = 0.1$ mol dm^{-3}, different mode of stirring and initial concentration of lithium ions. The initial concentrations of Li^+ are indicated: M correspond to mol dm^{-3}, MAG—magnetic stirring, MECH—mechanical stirring. The quantification of the relative amounts of calcite and vaterite was determined by X-ray diffraction analysis.

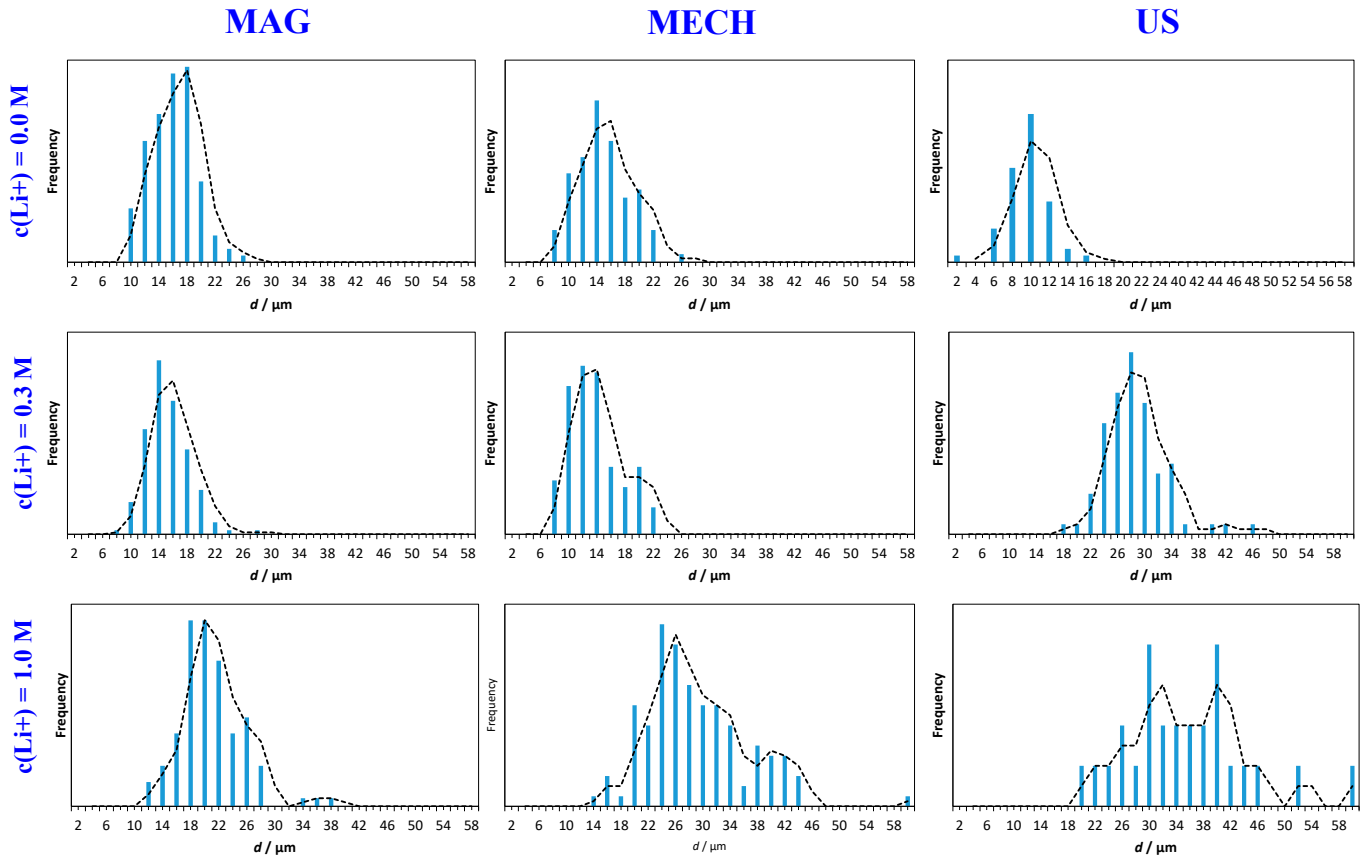

Figure 2. Particle size distribution of calcite crystals obtained after 5 days in the systems with different stirring modes (MECH—mechanical stirring, MAG—magnetic stirring, US—ultrasonic stirring) and initial Li^+ concentrations. Distributions were determined by using ImageJ.

3.3. Morphology

The morphology of the precipitate, predominantly calcite, was obtained after five days in the systems in which the mode of initial mixing and the concentration of added Li^+ was observed by scanning electron microscopy (Figure 3). Thus, the calcite crystals obtained in the model system (no lithium ions) for all three stirring modes and after five days of aging are the rhombohedrons with well-expressed {104} faces: the crystals in the MECH and MAG systems are more aggregated. However, the increasing Li^+ concentration caused a gradual change of dominant shape of crystals: in the systems with the lowest Li^+ concentration applied, $c(Li^+)$ = 0.1 mol dm^{-3}, prismatic calcite crystals with triangular faces and {001} truncations on the rhombohedral crystals can be observed. Indeed, crystal truncations and formation of triangular {001} faces at the expense of {104} rhombohedral face is expected under lower Li^+/Ca^{2+} concentration ratio [19]. The tendency of truncation of rhombohedrons at moderate lithium concentrations, $c(Li^+)$ = 0.3 mol dm^{-3} and 0.5 mol dm^{-3}, can be observed particularly in the MECH agitation mode, while in the MAG system they appear in a mixture with hexagonal plate-like crystals. Predominantly plate-like crystals have been obtained only in the US system. These crystals exhibit hexagonal morphology characterized by basal {001} face and {104} side faces, which is caused by predominant Li^+ adsorption on growing {104} faces. Consequently, the basal {001} faces are formed by truncation of all six {104} rhombohedral faces, thus resulting in specific plate-like crystal shape [44]. At the highest Li^+ concentrations applied, $c(Li^+)$ = 1.0 mol dm^{-3}, a mixture of plate-like and rhombohedral truncated crystals can still be observed in MECH systems, while in MAG and US systems only plate-like crystals predominates. The plate-like crystals obtained at highest Li^+ addition, typically show

macro-steps on the {001} faces, which has not been observed in systems with lower lithium concentrations.

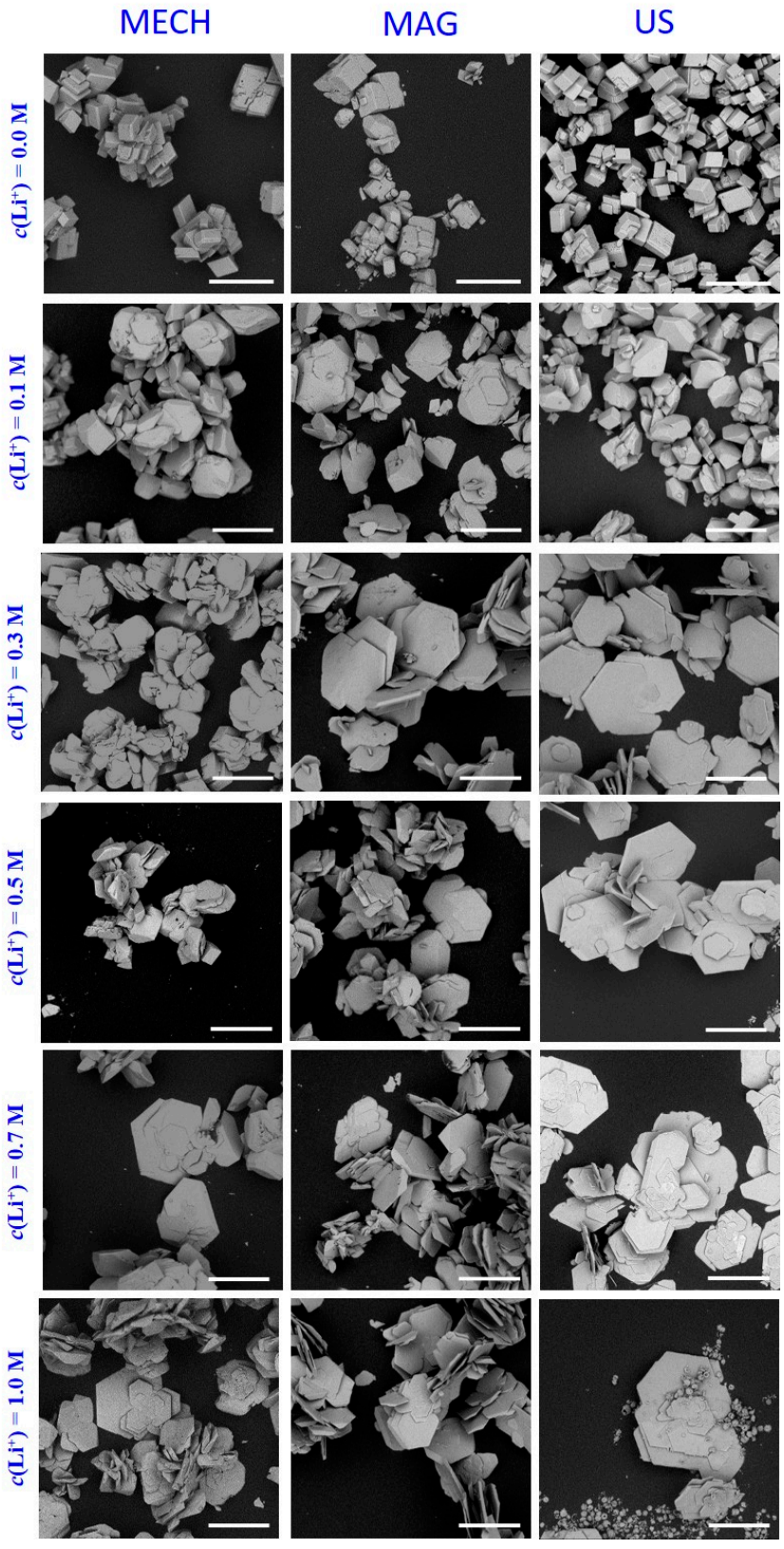

Figure 3. Morphologies of precipitates isolated after 5 days of aging in the systems with different initial stirring modes (MAG—magnetic, MECH—mechanical, US—ultrasonic irradiation) and different initial Li^+ concentrations, determined by SEM. Scale bars correspond to 30 μm.

The content of Li^+ incorporated into the calcite crystals isolated after five days of aging in systems with different initial LiCl concentrations is shown in Figure 4. It could be seen that the content of incorporated Li^+ almost linearly increases with increasing LiCl concentration in the solution for the applied mode of stirring. In addition, the amount of Li^+ is systematically the highest in the MECH and the lowest in the US system, which correlates with the observed morphological differences of precipitated calcite crystals. Indeed, the content of the rhombohedral and truncated crystals is the highest in the MECH systems and the lowest in the US, as well as that the thinnest crystals could be observed in the US systems. All these observations implicate that the growth of hexagonal {001} faces is inhibited by predominant Li^+ adsorption, so the incorporation is predominantly possible into the growing {104} faces. However, it should be emphasized that the amount incorporated in the US system aged at the highest LiCl concentration, c = 1.0 mol dm^{-3}, is disproportionately higher, which is a consequence of the vaterite still present in the suspension after five days. Microporous vaterite can absorb/adsorb a significant amount of solution as shown before [50,51].

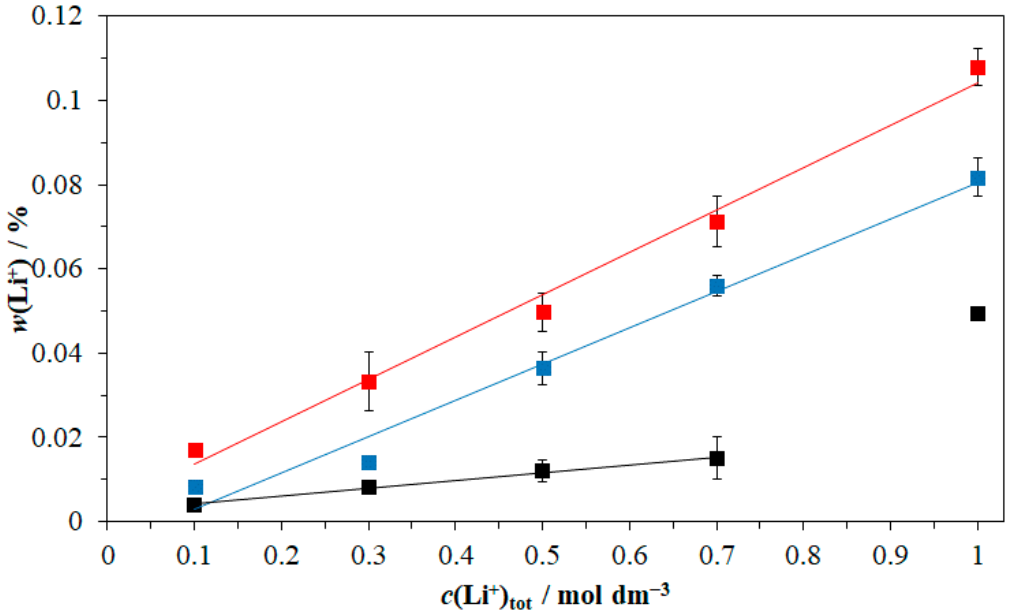

Figure 4. Amount of lithium incorporated in precipitate separated after 5 days of aging in the systems with different initial stirring modes (mechanical mixing (red line), magnetic mixing (blue line) and ultrasonic irradiation (black line)) and different initial Li^+ concentrations.

3.4. Precipitation Kinetics

The structural and morphological analyses of the precipitate sampled during the aging process of five days showed that initially a mixture of polymorphs and amorphous phase appeared. Indeed, the MECH and MAG samples isolated after the initial stirring (one hour) were typically aggregated vaterite particles, which subsequently transformed into the stable calcite after five days. Similarly, in the US systems and after 15 min of initial agitation, well dispersed vaterite particles, which subsequently transformed into the calcite, were observed (Figure S11).

The course of the precipitation reactions in the magnetically stirred precipitation systems with equimolar initial concentrations of reactants ($c_i(CaCl_2)$ = $c_i(NaHCO_3)$ = 0.1 mol dm^{-3}) and different lithium addition (0.0 mol dm^{-3} < c_i(LiCl) < 0.3 mol dm^{-3}) were followed by continuous measuring the pH. The experiments were conducted under magnetical stirring in which, compared to the MECH and US system, the highest initial vaterite was obtained. Figure 5 shows the representative progress curves, typical for solution-mediated transformation process [34,41,42], in which pH rapidly drops and reaches approximately constant value. Figure S12 shows

the respective concentration changes calculated from measured pH, for system with no LiCl addition. After some time, the additional drop occurs, thus indicating the establishment of the equilibrium for the stable phase (solubility). Significant prolongation of establishment of the equilibrium state can be observed in the systems with increasing Li^+ concentration. In the case of 0.3 mol dm^{-3} Li^+, the last step can be observed after approximately 18 h. However, the insert in the Figure 5 and Figure S12 shows that during the initial period, a step appeared as well. The dashed lines in the graphs correspond, from the top to bottom, to calculated values of solubility of: precursor, amorphous calcium carbonate ((c_s(acc) = 0.0900 mol dm^{-3}) ≙ (pH = 7.03)), metastable vaterite ((c_s(vat) = 0.0630 mol dm^{-3}) ≙ (pH = 5.99)) and stable calcite ((c_s(cal) = 0.0575 mol dm^{-3}) ≙ (pH = 5.682)). During the first stage of the process, which last about 150 s (from 0.1000 mol dm^{-3} to c_s(acc)) nucleation and growth of all phases, as well as aggregation, occur. Indeed, dissolution of amorphous calcium carbonate occurred below c_s(acc), but this process is rather fast and detectable only as a shoulder on the progress curve. During the second stage which last from about 150 s to 1500 s, concentration rapidly drop to values of vaterite solubility ((c_s(vat) = 0.0630 mol dm^{-3}) ≙ (pH = 5.99) and processes of vaterite and calcite growth are dominant. The third stage (from about 1500 s to 10,000 s) can be observed as a slow change of solution pH and concentration (concentration plateau), which is a consequence of two processes going on simultaneously: vaterite dissolution and calcite growth.

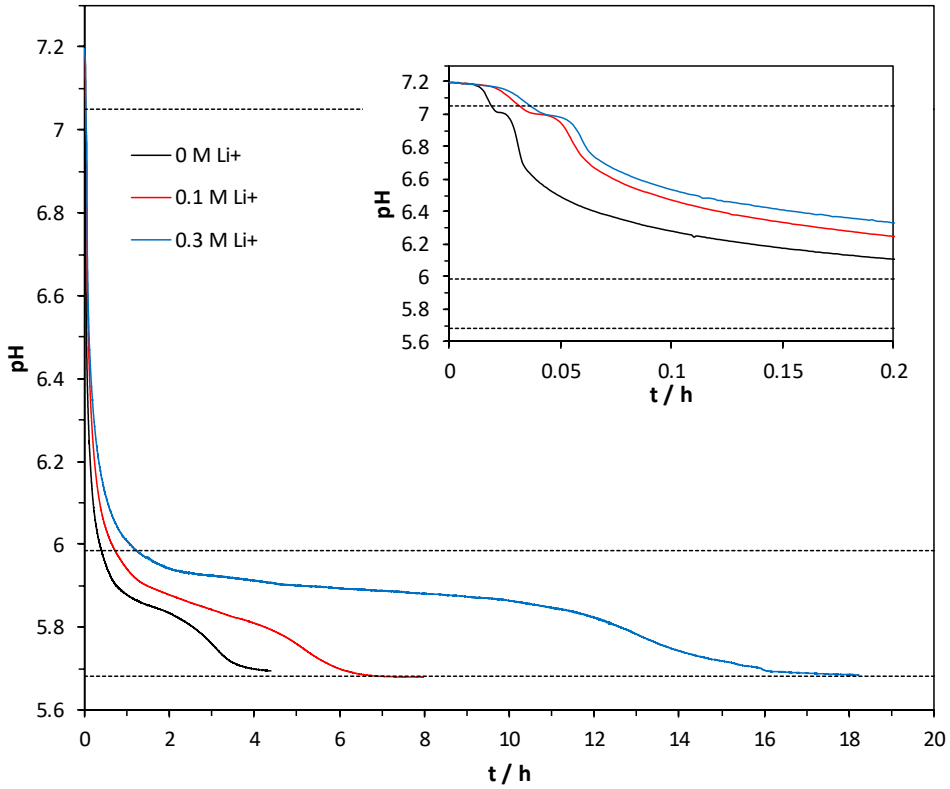

Figure 5. Progress curves, pH vs time of spontaneous precipitation of calcium carbonate: $c_i(CaCl_2) = c_i(NaHCO_3)$ = 0.1 mol dm^{-3} and different concentrations of LiCl initially present in the systems. The insert shows the pH changes during the initial 12 min of the process.

The last period of the transformation process started after complete disappearance of the vaterite so the calcite growth is an only process in the precipitation system. This period could be observed as a final step of the progress curve at about 2.5, 4.5 and 11.5 h and subsequent approach to equilibrium for calcite ((c_s(cal) = 0.0630 mol dm^{-3}) ≙ (pH = 5.69)). In order to understand the influence of Li^+ addition on the overall kinetics of vaterite to calcite transformation and corresponding morphological properties of calcite crystals

obtained in the presence of LiCl, additional kinetic measurements of the elementary precipitation process have been performed. Therefore, the crystal growth of vaterite and calcite seed, as well as dissolution of vaterite seed have been analyzed in the precipitation systems similar to those in which vaterite to calcite transformation occurred and which contained a limited range of LiCl concentrations, 0. 0 mol dm^{-3} < c(LiCl) < 0. 3 mol dm^{-3}. Figure 6 shows the progress curves, c *vs* time, for calcite and vaterite growth and for a range of LiCl concentrations: in both systems the initial concentration was 0.075 mol dm^{-3}, while the mass of calcite seed was 125 mg dm^{-3} and of vaterite seed was 1000 or 500 mg dm^{-3}. It could be seen that the increasing concentration of LiCl, slow down the calcite growth, while the growth of vaterite was not significantly affected. It should be emphasized that the solubility of each polymorphs was virtually identical for the range of applied LiCl concentrations (c_s(cal) = 0.0575 mol dm^{-3} and c_s(vat) = 0.0630 mol dm^{-3}). Figure 6 also shows the progress curves for vaterite dissolution in the presence of different concentrations of LiCl and c_i = 0.0575 mol dm^{-3}. It is evident that the LiCl addition in the applied range didn't significantly influence the dissolution kinetics. The growth rates of vaterite and calcite have been calculated from known initial mass of respective crystal seed, the average initial size of particles and measured changes of concentration of dissolved calcium carbonate. They have been expressed as the changes of linear dimensions of calcite or vaterite crystals for a given period of time, dl/dt, which is in the case of calcite the length of crystal edge, or radius of the vaterite particle (Figures S13 and S14). Different crystal growth or dissolution mechanisms (bulk diffusion, screw dislocation, surface nucleation) have been tested by correlating the rate with different expressions for supersaturation or undersaturation (Equations (2) and (4)–(6)). Figure 7 shows that the best linear fits for calcite and vaterite growth have been obtained for the so-called screw dislocation mechanism, $dl/dt = k\ (S - 1)\ \ln S$, where $S = (c/c_S)$. The rate constants calculated from the slope, k_{ln}, (Table 1) indicate that Li^+ ions do not change the controlling growth mechanisms, as well as they do not significantly influence the rate of vaterite growth. On the other hand, the growth of calcite is clearly inhibited. In addition, Figure 7 also shows that the vaterite dissolution is controlled by the diffusion of constituent ions from the surface into the bulk. Indeed, the observed predominant growth and dissolution mechanisms are consistent with some previous results on investigation of precipitation kinetics of calcium carbonate polymorphs in model systems of much lower initial supersaturations and in the absence of lithium ions [34,41,42]. The consistency of the measurements has been verified by varying the initial mass of crystal seed and satisfactory results have been obtained: typically, the rate constants changed for no more than ±5%. However, if the experimental results of vaterite transformation in the presence of Li^+ (Figure 5 and Figure S12) are compared with the kinetic data of calcite and vaterite crystal growth and dissolution determined in the independent set of seeding experiment (Table 1), consistency can be observed. Specifically, the vaterite growth and dissolution are not significantly affected by the addition and increase of Li^+, as could be observed from the values of respective rate constants.

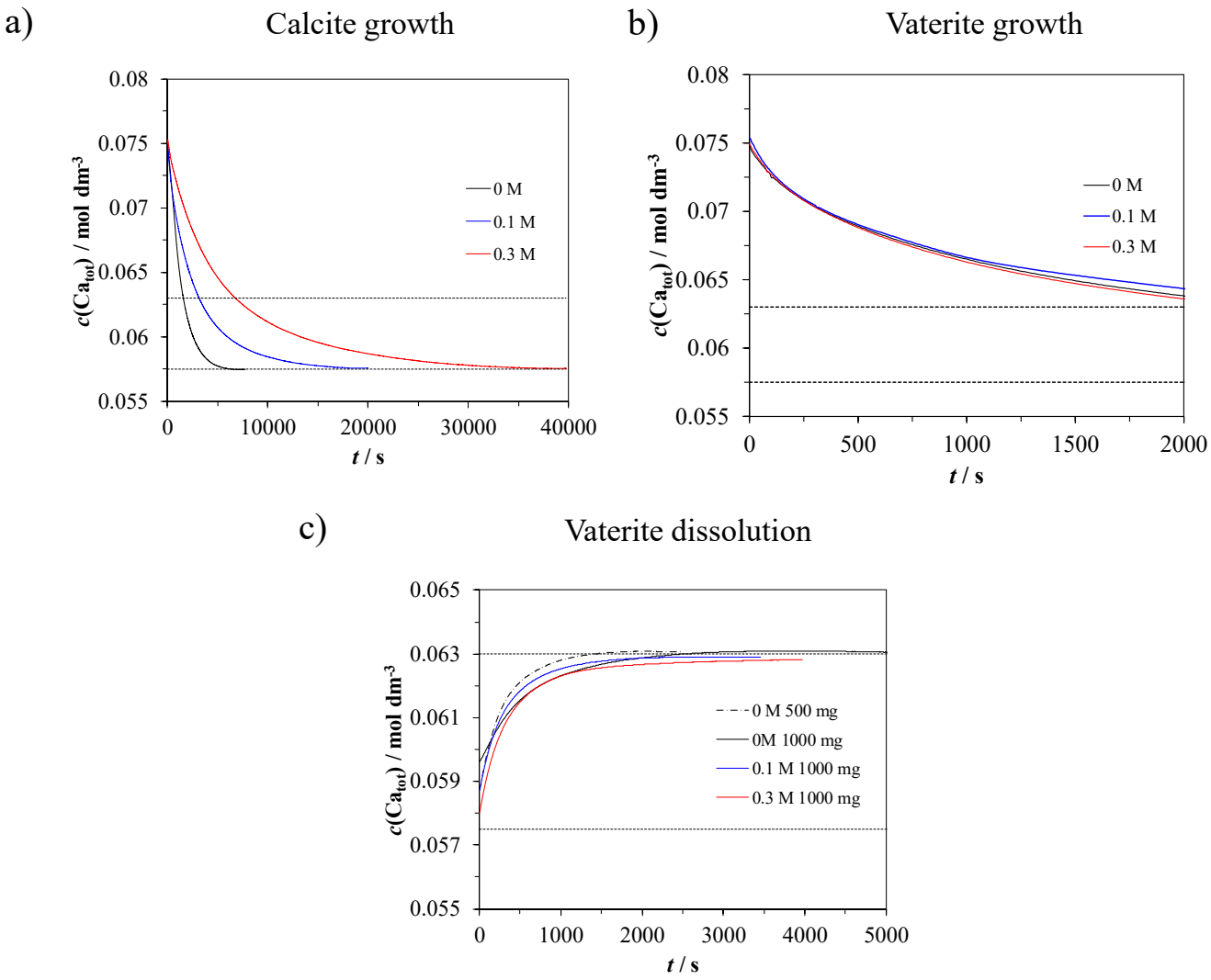

Figure 6. Progress curves, solution concentration vs. time of seeded growth of (**a**) calcite or (**b**) vaterite: $c_i(CaCl_2) = c_i(NaHCO_3) = 0.1$ mol dm^{-3} and different concentrations of LiCl initially present in the systems. (**c**) Dissolution of vaterite was initiated in the undersaturated system: $c_i(CaCl_2) = c_i(NaHCO_3) = 0.0575$ mol dm^{-3}. Initial mass concentrations of calcite and vaterite seed in the growth experiments were, γ(calcite) = 125 mg L^{-1} and γ(vaterite) = 125 mg L^{-1} while in dissolution experiments γ(vaterite) = 500 or 1000 mg L^{-1}.

Table 1. Calculated rate constants of calcite and vaterite grown in the systems, $c_i(CaCl_2) = c_i(NaHCO_3) = 0.1$ mol dm^{-3} and vaterite dissolution in the undersaturated system: $c_i(CaCl_2) = c_i(NaHCO_3) = 0.0575$ mol dm^{-3}, and different concentrations of LiCl initially present in the systems. Predominant mechanisms are growth on dislocation (k_{ln}) and diffusion of ions away from to surface into the bulk of solution (D).

$c(Li^+)$/mol dm^{-3}	Calcite Growth k_{ln}/μm s^{-1}	Vaterite Growth k_{ln}/μm s^{-1}	Vaterite Dissolution D/m^2 s^{-1}
0.00	20.4	37.9	3.4×10^{-9}
0.10	9.0	32.1	3.3×10^{-9}
0.30	4.8	32.1	2.9×10^{-9}

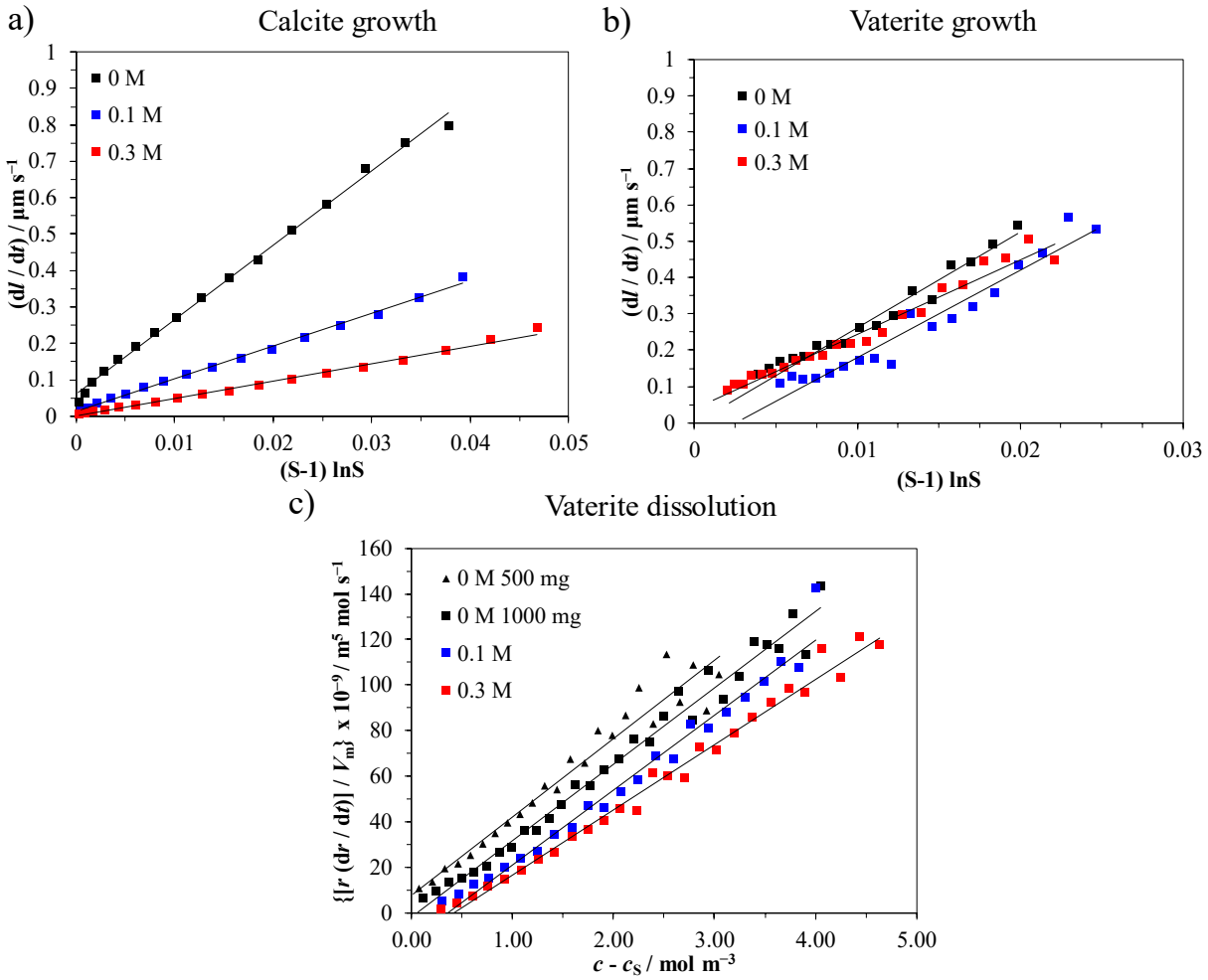

Figure 7. Plot of growth rates as a function of supersaturation expressed as $(S - 1)\ \ln S$, for (**a**) growth of calcite and (**b**) vaterite seed and (**c**) $c - c_S$ for the dissolution of vaterite, where c_s is solubility of respective polymorph and $S = (c/c_S)$. The mass concentrations or calcite and vaterite were, γ(calcite) = 125 mg L^{-1} and γ(vaterite) = 125 mg L^{-1} respectively. Plots correspond to data shown in Figure 6.

Only the calcite growth rate constants decrease from 20.4 µm s^{-1} at c(LiCl) = 0.0 mol dm^{-3} to 9.0 µm s^{-1} at c(LiCl) = 0.1 mol dm^{-3} and 4.8 µm s^{-1} at c(LiCl) = 0.3 mol dm^{-3}, which qualitatively correspond to prolongation of respective transformation process from 2.5 to 4.5 and 12.5 h.

4. Conclusions

This research aimed to investigate the role of different experimental parameters on the formation of uniform plate-like calcite crystal with the expressed {001} surfaces, in the systems in which precipitation has been initiated by fast mixing the equimolar CaCl2 and NaHCO3 solutions (ci = 0.10 mol dm^{-3}). For this purpose, different hydrodynamics (mode of stirring of the reaction components by magnetic stirring bar (MAG), mechanical paddle (MECH) or ultrasonic irradiation (US)) and the addition of Li+ in a wide concentration range, 0.0 mol dm^{-3} < c(Li+) < 1.0 mol dm^{-3} have been applied. In addition, the kinetics of solution mediated transformation of initially formed metastable polymorph, vaterite, has been followed in order to reproducibly describe the formation of plate-like calcite. The result showed that after 5 days of aging of the suspension, predominantly plate-like calcite has precipitated in the US system when the concentration of lithium ions was equal or higher than 0.3 mol dm^{-3}, while in the MECH and MAG systems concentration has been as high as 1.0 mol dm^{-3}. When the concentration of Li+ was lower than critical, truncated rhombohedral calcite crystals in a mixture with plate-like crystals have been obtained in

all systems. The chemical analysis of calcite obtained after aging period, showed that the highest Li+ incorporation was obtained in the MECH system, while the lowest was in the US systems, which correlate with a portion of truncated rhombohedrons in the mixture with plate-like crystals. The kinetics of vaterite to calcite transformation was found to extend with increasing Li+ concentration, but also depend on the mode of stirring: in the MAG and US systems traces of vaterite could be found even after 5 days when the c(Li+) = 1.0 mol dm^{-3}, while in the MECH system of the same concentration transformation is completed after two days. The analysis of the kinetics of the elementary precipitation processes involved in solution-mediated transformation indicates that the crystal growth and dissolution of vaterite are virtually not influenced by the Li+ addition, while the calcite growth is significantly inhibited, which prolonged the overall transformation.

Consequently, the optimal experimental protocol for preparation of regular plate-like calcite crystals with expressed {001} surfaces and from equimolar CaCl2 and NaHCO3 solutions (ci = 0.10 mol dm^{-3}), implicit the initial US agitation and the addition of LiCl, c = 0.3 mol dm^{-3}. Thus obtained crystals contain no macro-steps and are uniform in size.

Supplementary Materials: The following are available online at https://www.mdpi.com/2073-4352/11/3/250/s1, Table S1. A brief derivation of Equations (4)–(6); Figure S1: FTIR spectra of the precipitates obtained in the magnetically stirred (MAG) precipitation systems; Figure S2: FTIR spectra of the precipitates obtained in the mechanically stirred (MAG) precipitation systems; Figure S3: FTIR spectra of the precipitates obtained in the ultrasonicated (US) precipitation systems; Table S2: Assignment of IR bands in FTIR spectra of precipitates obtained after 5 days of aging; Table S3: Polymorphic composition of $CaCO_3$ samples obtained by different stirring modes; Figure S4: PXRD diffractograms of the $CaCO_3$ precipitates obtained in the ultrasonicated (US) precipitation systems; Figure S5: PXRD diffractograms of the $CaCO_3$ precipitates obtained in the mechanically stirred and magnetically stirred precipitation systems; Table S4: Assignment of peaks in PXRD patterns of all samples; Figure S6: Particle size distribution of calcium carbonate samples obtained in the magnetically stirred (MAG) precipitation systems; Figure S7: Particle size distribution of calcium carbonate samples obtained in the mechanically stirred (MECH) precipitation systems; Figure S8: Particle size distribution of calcium carbonate samples obtained in the ultrasonicated (US) precipitation systems; Figure S9: Comparison of particle size distribution of calcium carbonate samples; Figure S10: The average particle sizes of calcite crystals; Figure S11: Scanning electron micrographs of calcium carbonate samples; Figure S12 Progress curve, solution concentration vs. time, of the spontaneous precipitation and transformation of calcium carbonate. Figure S13. Change of the initial length (lo = 1 μm) of calcite crystal edge (a) and the radius of the vaterite particle (b) vs. time in the crystal growth experiments; Figure S14. Plot of growth rates (dl/dt) as a function of time for the calcite (a) and vaterite (b) crystal growth experiments.

Author Contributions: Conceptualization, D.K.; methodology, D.K. and N.M.M.; validation, D.K. and N.M.M.; formal analysis, N.M.M., J.K., B.N.D. and D.K.; investigation, N.M.M., J.K. and B.N.D.; resources, D.K. and G.F.; data curation, N.M.M.; writing—original draft preparation, N.M.M., J.K. and D.K.; writing—review and editing, D.K.; visualization, D.K. and N.M.M.; supervision, D.K. and G.F.; project administration, D.K.; funding acquisition, D.K. and G.F. All authors have read and agreed to the published version of the manuscript.

Funding: This research received no external funding.

Data Availability Statement: Data is contained within the article or supplementary material.

Acknowledgments: This work has been supported in part (N.M., J.K., B.N.D. and D.K.) by Croatian Science Foundation under the project (IP-2013-11-5055).

Conflicts of Interest: The authors declare no conflict of interest.

References

1. Matijaković, N.; Magnabosco, G.; Scarpino, F.; Fermani, S.; Falini, G.; Kralj, D. Synthesis and Adsorbing Properties of Tabular {001} Calcite Crystals. *Crystals* **2019**, *9*, 16. [CrossRef]
2. Ukrainczyk, M.; Kontrec, J.; Kralj, D. Precipitation of different calcite crystal morphologies in the presence of sodium stearate. *J. Colloid Interface Sci.* **2009**, *329*, 89–96. [CrossRef]

3. Stepić, R.; Jurković, L.; Klementyeva, K.; Ukrainczyk, M.; Grdičak, M.; Smith, D.M.; Kralj, D.; Smith, A.S. Adsorption of Aspartate Derivatives to Calcite Surfaces in Aqueous Environment. *Cryst. Growth Des.* **2020**, *20*, 2853–2859. [CrossRef]
4. Orme, C.A.; Noy, A.; Wierzbicki, A.; Mcbride, M.T.; Grantham, M.; Teng, H.H.; Dove, P.M.; Deyoreo, J.J. Formation of chiral morphologies through selective binding of amino acids to calcite surface steps. *Nature* **2001**, *411*, 775–779. [CrossRef]
5. Davis, K.J.; Dove, P.M.; De Yoreo, J.J. The role of Mg^{2+} as an impurity in calcite growth. *Science* **2000**, *290*, 1134–1137. [CrossRef] [PubMed]
6. De Yoreo, J.J.; Vekilov, P.G. Principles of Crystal Nucleation and Growth. *Rev. Mineral. Geochem.* **2003**, *54*, 57–93. [CrossRef]
7. Mann, S. *Biomineralization: Principles and Concepts in Bioinorganic Materials Chemistry*; Oxford University Press on Demand: New York, NY, USA, 2001; ISBN 0198508824.
8. Mann, S. Molecular recognition in biomineralization. *Nature* **1988**, *332*, 119–124. [CrossRef]
9. Rani, R.S.; Saharay, M. Molecular dynamics simulation of protein-mediated biomineralization of amorphous calcium carbonate. *RSC Adv.* **2019**, *9*, 1653–1663. [CrossRef]
10. Chen, T.; Shi, P.; Li, Y.; Duan, T.; Yu, Y.; Li, X.; Zhu, W. Biomineralization of varied calcium carbonate crystals by the synergistic effect of silk fibroin/magnesium ions in a microbial system. *CrystEngComm* **2018**, *20*, 2366–2373. [CrossRef]
11. de Carvalho, R.T.; Salgado, L.T.; Amado Filho, G.M.; Leal, R.N.; Werckmann, J.; Rossi, A.L.; Campos, A.P.C.; Karez, C.S.; Farina, M. Biomineralization of calcium carbonate in the cell wall of Lithothamnion crispatum (Hapalidiales, Rhodophyta): Correlation between the organic matrix and the mineral phase. *J. Phycol.* **2017**, *53*, 642–651. [CrossRef] [PubMed]
12. Njegić-Džakula, B.; Brečević, L.; Falini, G.; Kralj, D. Kinetic Approach to Biomineralization: Interactions of Synthetic Polypeptides with Calcium Carbonate Polymorphs. *Croat. Chem. Acta* **2011**, *84*, 301–314. [CrossRef]
13. Addadi, L.; Weiner, S. Interactions between acidic proteins and crystals: Stereochemical requirements in biomineralization. *Proc. Natl. Acad. Sci. USA* **1985**, *82*, 4110–4114. [CrossRef] [PubMed]
14. Falini, G.; Fermani, S.; Goffredo, S. Coral biomineralization: A focus on intra-skeletal organic matrix and calcification. *Semin. Cell Dev. Biol.* **2015**, *46*, 17–26. [CrossRef]
15. Yang, M.; Stipp, S.L.S.; Harding, J. Biological control on calcite crystallization by polysaccharides. *Cryst. Growth Des.* **2008**, *8*, 4066–4074. [CrossRef]
16. Freeman, C.L.; Harding, J.H.; Quigley, D.; Rodger, P.M. Simulations of ovocleidin-17 binding to calcite surfaces and its implications for eggshell formation. *J. Phys. Chem. C* **2011**, *115*, 8175–8183. [CrossRef]
17. Aizenberg, J.; Hendler, G. Designing efficient microlens arrays: Lessons from Nature. *J. Mater. Chem.* **2004**, *14*, 2066–2072. [CrossRef]
18. Ye, X.; Zhang, F.; Ma, Y.; Qi, L. Brittlestar-inspired microlens arrays made of calcite single crystals. *Small* **2015**, *11*, 1677–1682. [CrossRef]
19. Rajam, S.; Mann, S. Selective stabilization of the (001) face of calcite in the presence of lithium. *J. Chem. Soc. Chem. Commun.* **1990**, 1789–1791. [CrossRef]
20. Pastero, L.; Aquilano, D.; Costa, E.; Rubbo, M. 2D epitaxy of lithium carbonate inducing growth mechanism transitions on {0 0 0 1}-K and {0 1 $\bar{1}$ 8}-S forms of calcite crystals. *J. Cryst. Growth* **2005**, *275*, 1625–1630. [CrossRef]
21. Pastero, L.; Aquilano, D. $CaCO_3$ (Calcite)/Li2CO_3 (zabuyelite) anomalous mixed crystals. Sector zoning and growth mechanisms. *Cryst. Growth Des.* **2008**, *8*, 3451–3460. [CrossRef]
22. Kitano, Y. The Behavior of Various Inorganic Ions in the Separation of Calcium Carbonate from a Bicarbonate Solution. *Bull. Chem. Soc. Jpn.* **1962**, *35*, 1973–1980. [CrossRef]
23. Titiloye, J.O.; Parker, S.C.; Osguthorpe, D.J.; Mann, S. Predicting the influence of growth additives on the morphology of ionic crystals. *J. Chem. Soc. Chem. Commun.* **1991**, 1494–1496. [CrossRef]
24. Pastero, L.; Costa, E.; Bruno, M.; Rubbo, M.; Sgualdino, G.; Aquilano, D. Morphology of calcite ($CaCO_3$) crystals growing from aqueous solutions in the presence of Li+ ions. Surface behavior of the {0001} form. *Cryst. Growth Des.* **2004**, *4*, 485–490. [CrossRef]
25. Bruno, M.; Massaro, F.R.; Prencipe, M.; Aquilano, D. Surface reconstructions and relaxation effects in a centre-symmetrical crystal: The {00.1} form of calcite ($CaCO_3$). *CrystEngComm* **2010**, *12*, 3626–3633. [CrossRef]
26. Song, R.Q.; Cölfen, H. Additive controlled crystallization. *CrystEngComm* **2011**, *13*, 1249–1276. [CrossRef]
27. Titiloye, J.O.; Parker, S.C.; Mann, S. Atomistic simulation of calcite surfaces and the influence of growth additives on their morphology. *J. Cryst. Growth* **1993**, *131*, 533–545. [CrossRef]
28. Ukrainczyk, M.; Stelling, J.; Vučak, M.; Neumann, T. Influence of etidronic acid and tartaric acid on the growth of different calcite morphologies. *J. Cryst. Growth* **2013**, *369*, 21–31. [CrossRef]
29. Enomoto, N.; Sung, T.-H.; Nakagawa, Z.-E.; Lee, S.-C. Effect of ultrasonic waves on crystallization from a supersaturated solution of alum. *J. Mater. Sci.* **1992**, *27*, 5239–5243. [CrossRef]
30. Choi, H.L.; Enomoto, N.; Nakagawa, Z.E. Effect of ultrasonic irradiation on precipitation of lead oxalate from aqueous solution. *J. Mater. Sci.* **1994**, *29*, 3239–3242. [CrossRef]
31. Boyjoo, Y.; Pareek, V.K.; Liu, J. Synthesis of micro and nano-sized calcium carbonate particles and their applications. *J. Mater. Chem. A* **2014**, *2*, 14270–14288. [CrossRef]
32. Štajner, L.; Kontrec, J.; Njegić Džakula, B.; Maltar-Strmečki, N.; Plodinec, M.; Lyons, D.M.; Kralj, D. The effect of different amino acids on spontaneous precipitation of calcium carbonate polymorphs. *J. Cryst. Growth* **2018**, *486*, 71–81. [CrossRef]

33. Njegić-Džakula, B.; Falini, G.; Brečević, L.; Skoko, Ž.; Kralj, D. Effects of initial supersaturation on spontaneous precipitation of calcium carbonate in the presence of charged poly-l-amino acids. *J. Colloid Interface Sci.* **2010**, *343*, 553–563. [CrossRef] [PubMed]
34. Kralj, D.; Brečević, L.; Kontrec, J. Vaterite growth and dissolution in aqueous solution II. Kinetics of transformation. *J. Cryst. Growth* **1997**, *177*, 248–257. [CrossRef]
35. Fermani, S.; Njegić-Džakula, B.; Reggi, M.; Falini, G.; Kralj, D. Magnesium and temperature control on aragonite crystal aggregation and morphology. *CrystEngComm* **2017**, *19*, 2451–2455. [CrossRef]
36. Kelly, D.R.; Harrison, S.J.; Jones, S.; Masood, M.A.; Morgan, J.J.G. Rapid crystallisation using ultrasonic irradiation—sonocrystallisation. *Tetrahedron Lett.* **1993**, *34*, 2689–2690. [CrossRef]
37. Dalas, E. The effect of ultrasonic field on calcium carbonate scale formation. *J. Cryst. Growth* **2001**, *222*, 287–292. [CrossRef]
38. Njegić Džakula, B.; Kontrec, J.; Ukrainczyk, M.; Sviben, S.; Kralj, D. Polymorphic composition and morphology of calcium carbonate as a function of ultrasonic irradiation. *Cryst. Res. Technol.* **2014**, *49*, 244–256. [CrossRef]
39. Rasband, W. Image J Image Processing and Analysis in Java. Available online: https://ui.adsabs.harvard.edu/abs/2012ascl.soft06013R/abstract (accessed on 26 February 2021).
40. Ukrainczyk, M.; Kontrec, J.; Babić-Ivančić, V.; Brečević, L.; Kralj, D. Experimental design approach to calcium carbonate precipitation in a semicontinuous process. *Powder Technol.* **2007**, *171*, 192–199. [CrossRef]
41. Kralj, D.; Brečević, L.; Nielsen, A.E. Vaterite Growth and Dissolution in Aqueous Solution II. Kinetics of disolution. *J. Cryst. Growth* **1994**, *143*, 269–276. [CrossRef]
42. Kralj, D.; Brečević, L.; Nielsen, A.E. Vaterite growth and dissolutionin aqueous solution I. Kinetics of crystal growth. *J. Cryst. Growth* **1990**, *104*, 793–800. [CrossRef]
43. Brečević, L.; Kralj, D. *Kinetics and Mechanisms of Crystal Growth in Aqueous Systems*; Kallay, N., Ed.; Marcel Dekker, Inc.: New York, NY, USA, 2000.
44. Aquilano, D.; Pastero, L. Anomalous mixed crystals: A peculiar case of adsorption/absorption. *Cryst. Res. Technol.* **2013**, *48*, 819–839. [CrossRef]
45. Brečević, L.; Kralj, D.; Garside, J. Factors influencing the distibution of hydrates in calcium oxalate precipitation. *J. Cryst. Growth* **1989**, *97*, 460–468. [CrossRef]
46. Stanković, A.; Kontrec, J.; Džakula, B.N.; Kovačević, D.; Marković, B.; Kralj, D. Preparation and characterization of calcium oxalate dihydrate seeds suitable for crystal growth kinetic analyses. *J. Cryst. Growth* **2018**, *500*, 91–97. [CrossRef]
47. Hem, S.L. The effect of ultrasonic vibrations on crystallization processes. *Ultrasonics* **1967**, *5*, 202–207. [CrossRef]
48. Luque De Castro, M.D.; Priego-Capote, F. Ultrasound-assisted crystallization (sonocrystallization). *Ultrason. Sonochem.* **2007**, *14*, 717–724. [CrossRef] [PubMed]
49. Patel, M.A.; Bhanvase, B.A.; Sonawane, S.H. Production of Cerium Zinc Molybdate Nano Pigment by Innovative Ultrasound-Assisted Approach. *Ultrason. Sonochem.* **2013**, *20*, 906–913. [CrossRef]
50. Beck, R.; Andreassen, J.P. Spherulitic growth of calcium carbonate. *Cryst. Growth Des.* **2010**, *10*, 2934–2947. [CrossRef]
51. Andreassen, J.P. Formation mechanism and morphology in precipitation of vaterite—Nano-aggregation or crystal growth? *J. Cryst. Growth* **2005**, *274*, 256–264. [CrossRef]